

## Scale effects in physical modelling of a generalized OWC

Antonino Viviano\*, Stefania Naty, Enrico Foti

Department of Civil Engineering and Architecture, University of Catania, via S. Sofia 64, 95123, Catania, Italy



### ARTICLE INFO

#### Keywords:

Oscillating water column  
Experiments  
Natural oscillation period  
Wave reflection  
Loadings

### ABSTRACT

Physical modelling is extensively applied in the study of Oscillating Water Column (OWC) devices since it furnishes a reliable evaluation of nonlinear effects, as those induced by the interaction between surface waves and air inside the pneumatic chamber. In this paper, a small scale generalized device is compared to a similar large scale model under random waves, in order to evaluate the main scaling issues on (i) hydrodynamics of the water column, (ii) wave reflection and (iii) loadings at the outer front wall. The small scale model tested allowed to investigate the effects of air compressibility as well.

Natural oscillation period is analysed first, which is obtained from the delay between the oscillating motions inside the device and those outer the front wall. Such a period increases in the small scale with the height of the chamber due to the “spring” effect of the air compressibility. Furthermore, the downscale of the OWC causes a reduction of the reflection coefficient, which is in part recovered by increasing the height of the device. Extreme loadings on the front wall can be underestimated by the small scale but safe conditions are always achieved for the high-chamber model.

### 1. Introduction

Operation of Wave Energy Converters (WECs) involves the interaction of sea water waves with fixed and moving structural components. In OWC devices, such an interaction is characterized by the presence of air which is alternately compressed and decompressed by waves inside a pneumatic chamber and is forced to flow through an air turbine. Falcao and Henriques (2016) noted that the absence of moving components inside the sea makes OWC devices the simplest and the most extensively analysed type of WECs.

Recent studies on OWC devices analysed their performances both in oceans and in semi-sheltered seas, by using empirical, numerical or physical modelling approaches. In particular, Carballo and Iglesias (2012) and Lopez et al. (2016) considered a site located in A Guarda (Galicia, NW Spain), along the Atlantic Ocean. The incident wave climate was summarized in a limited number of wave conditions, for which the OWC device was tested.

Lopez et al. (2016) carried out their tests by means of a validated RANS-VOF numerical model, which takes into account the non-linear hydrodynamic effects that take place in the process of conversion of wave power into pneumatic power. They found an optimum value of damping due to the Power Take Off (PTO), which causes an overall efficiency in the conversion from wave to pneumatic energy of 27.5%.

Regarding the optimization of OWC systems by means of physical modelling, several investigations have been already performed:

Mahnamfar and Altunkaynak (2016) investigated the influence of water depth and opening height; Mahnamfar and Altunkaynak (2017) studied the variation of the angle of the front plate; Rezanejad et al. (2017) tested the influence of the turbine damping; Vyzikas et al. (2017) examined four multi-chamber devices, with and without the PTO.

Naty et al. (2016) developed a feasibility study of an OWC device placed inside the coastal structure of a Mediterranean Port in Giardini Naxos (Italy), where only low wave energy levels are available (see Iuppa et al., 2015a; b). The optimization of the device was achieved by means of a small scale physical model in which the front wall submergence was varied. The pneumatic chamber measurements during such tests were considered for estimating PTO efficiency as a function of wave conditions. Those results were combined to the incident wave conditions, and allowed an overall performance of 18% for the case of study to be obtained. Furthermore, they found that the payback period of the investment is 19 years, although the site of the study is a sheltered zone for the energy conversion.

The performance of the OWC systems was recently investigated by Sheng and Lewis (2016), who considered the effect of air compressibility inside the pneumatic chamber, i.e. the so called “spring effect” which allows to store and release energy during a wave cycle. In particular, air compressibility was first linearized and further coupled with the hydrodynamics of the OWC. Both frequency-domain simulations and time-domain simulations were carried out, in order to achieve a complete understanding of the problems. They found that air

\* Corresponding author.

E-mail addresses: [antonino.viviano@dica.unict.it](mailto:antonino.viviano@dica.unict.it) (A. Viviano), [stefanianaty@virgilio.it](mailto:stefanianaty@virgilio.it) (S. Naty), [efoti@dica.unict.it](mailto:efoti@dica.unict.it) (E. Foti).

**Nomenclature**

$\Delta p$	wave pressure at the front opening of the chamber
$\delta$	orifice thickness
$\Gamma$	dimensionless group for air compressibility, see eq. (6)
$\hat{T}$	dimensionless resonance period of the device, see eq. (10)
$\mu$	dynamic viscosity
$\omega$	angular frequency of waves
$\rho$	density
$\varepsilon$	scale factor $L_M/L_m$
$a$	draft of front vertical wall
$A_w$	amplitude of waves
$B$	longitudinal width of chamber
$B_t$	transverse width of chamber
$C_r$	total reflection coefficient of a random wave train
$C_{r(f)}$	spectral reflection coefficient, defined for each wave component of the spectrum
$d$	water depth from chamber floor
$d_0$	orifice diameter
$F$	force acting on the front wall of the OWC caisson
$f$	generic wave frequency
$Fr$	Froude number
$g$	acceleration of gravity
$h$	water depth from flume floor
$H^*$	significant incident relative wave height = $H_{m0,i}/h$
$h_a$	height of the air volume inside the chamber in the still condition

$h_i$	opening height of front vertical wall
$h_t$	height of chamber
$H_{c,m0}$	significant (spectral) wave height inside the chamber
$H_{m0,i}$	significant (spectral) height of incident waves
$k$	polytropic exponent
$L$	characteristic length
$L_p$	wave length (in depth $h$ ) based upon peak period
$p$	relative pressure in chamber
$p_{at}$	atmospheric absolute pressure
$q$	flow rate driven by the interior water surface
$Re$	Reynolds number
$s$	approach slope
$s_w$	wave steepness
$T$	generic wave period
$T^*$	natural period of the device
$T_p$	peak wave period
$U$	characteristic velocity
$V$	air chamber volume

**Subscripts**

1/250	maximum value, equal to the average of 4 peaks from 1000 waves
$at$	atmospheric conditions
$M$	large scale model
$m$	small scale model

compressibility may significantly change the capacity of converting wave energy when the pneumatic chamber of the OWC is large enough.

Notwithstanding the numerical models allow to test quite easily devices having different geometries, physical models are often carried out because they provide reliable information on non-linear effects. In the physical modelling of OWC devices, Particle Imaging Velocimetry (PIV) is particularly useful since it furnishes velocity fields, kinetic energy and vorticity at the device (see Fleming et al., 2012; Mitchell Ferguson et al., 2017; Fleming and Macfarlane, 2017a). Furthermore, the inflow and outflow discharge coefficients at the PTO can be estimated, as in Fleming and Macfarlane (2017b). Such coefficients allows to achieve an accurate flow rate prediction and consequently a good prediction of the performance of the devices.

Usually, the physical model tests are carried out in small scales, due to the limits in the dimensions of laboratories. An exception is represented by the tests conducted on a generalized OWC at the Grosse Wellenkanal (GWK) in Hannover, Germany, by Allsop et al. (2014). Those tests (at approximately 1:5 to 1:9 of full scale) measured wave loads, water column movements, air pressures and flows through a number of PTOs, simulated by means of orifices. Viviano et al. (2016) analysed wave reflection and loadings on such a generalized device under random waves. In particular, forces at the OWC walls were compared with the available formulations for impulsive loading prediction; such comparisons showed significant underestimation for the heaviest incident wave conditions.

The problem of estimating the scale effects in WECs was recently recalled by Sheng et al. (2014), who developed a theoretical analysis and an explanation of some important scaling issues. In particular, they stated that the physical modelling is acceptable if the Reynolds number of the water particle velocity in waves is larger than  $10^5$ , i.e. when the viscous forces are negligible. Specifically for OWC devices, they showed that the volume of the pneumatic chamber must be scaled by a modified scale factor, in order to take into account the effect of air compressibility. A similar indication on the scaling of air chamber was also expressed by Falcao and Henriques (2014). Furthermore, Weber (2007) suggested to maintain the same air chamber height for every geometric

scale of the model, otherwise it should be provided an additional air volume.

In such a context, the present paper aims at investigating the scale effects on hydrodynamics and loadings at a small scale generalized OWC device, similar to that analysed by Viviano et al. (2016) in large scale tests. The paper is organized as follows: the definition of the scale factor is discussed in Section 2, together with the derivation of the main dimensionless parameters. Section 3 shows the setup of the small scale model, which allows to vary the pneumatic chamber height and to investigate the air compressibility effects. The results are reported and discussed in Section 4, by considering natural oscillation period of the water column, wave reflection and loadings at the outer front wall. Section 5 discusses the effects of air chamber volume on the wave motion and loading at the OWC. The conclusions are drawn in Section 6, by comparing the results obtained from models with different scales and pneumatic chambers.

**2. Dimensional analysis**

For a given physical problem, dimensional analysis allows to identify the fundamental parameters and dimensionless variables. Therefore, data obtained from a prototype and/or from physical models can be correlated each other on the basis of such parameters. Usually a physical model is geometrically similar to the full (or large) scale model. It is possible to define a scale factor  $\varepsilon$  equal to the ratio between a generic geometrical length at the large scale  $L_M$  model and the corresponding length at the small scale model  $L_m$ :

$$\varepsilon = \frac{L_M}{L_m} \quad (1)$$

On the basis of such a scale factor between lengths, the ratios between areas and between volumes can be obviously obtained geometrically as  $\varepsilon^2$  and  $\varepsilon^3$ , respectively.

Once the geometrical similarity is chosen, the physical phenomenon must be investigated in order to verify if all the dimensional quantities scale correctly in the larger (or prototype) and smaller models or if

some of them deviate. In the latter case, the phenomenon analysed in the small scale model may heavily differ from the large scale and a correction of the scale effect must be introduced.

The interaction between surface waves and OWC device involves the dynamics of two fluids, i.e. water and air, which mutually affect each other. A further grade of complexity is introduced by the presence of the power take off (PTO). Falcao and Henriques (2014) noticed that the dimensional analysis leads to a scale ratio of the power equal to  $\varepsilon^{7/2}$ ; indeed, a geometrical scale 1:10 implies a power ratio of about 1:3200. Such a ratio is too small for allowing an adequate modelling of the turbine, which is usually substituted by an orifice or by a layer of porous media.

The application of the dimensional analysis approach to continuity and Navier-Stokes equation for fluid dynamics leads to the definition of Froude number  $Fr$  and Reynolds number  $Re$  (Wilcox, 1997):

$$Fr = \frac{U}{\sqrt{gL}} \quad (2)$$

$$Re = \frac{\rho UL}{\mu} \quad (3)$$

where  $U$  is a characteristic speed of the fluid,  $L$  is a characteristic length of the system,  $g$  is the acceleration of gravity,  $\rho$  and  $\mu$  are the density and the viscosity, respectively. For water motion under waves, the characteristic speed  $U$  can be defined by employing the maximum water particle velocity from small-amplitude water wave theory (Dean and Dalrymple, 1991):

$$U = \omega A_w \quad (4)$$

where  $A_w$  is the amplitude and  $\omega$  is the angular frequency of the incoming waves ( $\omega = 2\pi/T$  with  $T$  the period on waves).

For the two dimensionless groupings introduced above, the physical meaning can be expressed as a balance between forces acting on the fluid: i)  $Fr$  provides a measure of the importance of inertial forces with respect to gravity forces; ii)  $Re$  compares the inertial forces and the viscous forces.

For a fixed scale ratio  $\varepsilon$  between lengths of large and small scale model, it is not possible to match both Froude and Reynolds numbers if the two models have the same fluids and acceleration of gravity. Indeed, from eq. (2) the ratio between large and small scale characteristic velocity is equal to  $\varepsilon^{0.5}$ . On the contrary, the matching of eq. (3) yields to a velocity scale factor  $\varepsilon^{-1}$ . As stated by Sheng et al. (2014), usually the Froude similarity alone is followed since it can ensure the correctness of model scaling under the condition of large Reynolds number, i.e.  $Re > 10^5$ .

The presence of the air inside the OWC chamber causes a further scaling issue which involves compressibility. The air varies its pressure over the time and flows into the PTO. On the basis of the mass continuity, the variation of the amount of air inside the chamber is due to its volume variation for a fixed density (i.e.  $\rho dV/dt$ ) and to the density variability for a fixed volume  $V d\rho/dt$ , where  $\rho$  and  $V$  are density and volume of the air into the OWC, respectively. The volume variation inside the chamber can be seen as the flow rate  $q$  of the water inside the OWC.

The density variation is due to the presence of air compression, which can be well represented inside the OWC chamber by means of the pressure-density relationship for a perfect gas:

$$\frac{p + p_{at}}{\rho^k} = \frac{p_{at}}{\rho_{at}^k} \quad (5)$$

where  $p$  is the relative pressure inside the chamber,  $p_{at}$  is the absolute pressure out of the OWC,  $\rho_{at}$  is the outer density,  $k$  is the polytropic exponent which is related to the turbine efficiency, as obtained in Falcao and Henriques (2014). The latter exponent assumes the maximum value 1.4 if the turbine is perfectly efficient and the flow is isentropic. On the contrary,  $k = 1$  for a turbine which has null efficiency,

since no work is done and the process is isothermal.

On the basis of eq. (5), it is possible to compare the air mass variability inside the OWC due to density and volume variation, thus obtaining the following dimensionless group:

$$\Gamma = \frac{V d\rho/dt}{\rho q} = \frac{V}{kq(p + p_{at})} \frac{dp}{dt} \quad (6)$$

Falcao and Henriques (2014) suggest that such a dimensionless group must be constant in order to achieve a full dynamic similarity between large and small scale models. The coefficient  $k$  depends on the PTO characteristics rather than on the geometric scale. Under the Froude similarity conditions, the scales of flow rate  $q$  and of pressure variation  $dp/dt$  are  $\varepsilon^{2.5}$  and  $\varepsilon^{0.5}$ , respectively. Furthermore,  $p_{at}$  are constant at different scales and the relative pressures inside the chamber  $p$  can be considered small when compared to absolute pressure (i.e.  $p \ll p_{at}$ ). All those considerations cause that the air volume should be scaled by  $\varepsilon^2$  in order to have a constant value of  $\Gamma$ , instead the geometric similarity yields the volume scale to  $\varepsilon^3$ , as highlighted by Sheng et al. (2014). For such a reason, Weber (2007) asserts that the scaling requirements of air compressibility can be satisfied by maintaining the air chamber height at all scales: in this way the ratio between volumes in the models at different scales coincide to the ratio of areas, i.e.  $\varepsilon^2$ . Unfortunately, such a scale distortion is often not achievable in small laboratories but it can be substituted with any increase of the chamber volume, for example by connecting the chamber with an air reservoir. In order to face such a scaling issue of the OWCs, another possible approach is to test the effect of a small variation of air volume, or specifically of the chamber height, so carrying out a sensitivity analysis. Such a method may allow to overcome the need for a great air volume reservoir, since the results from two small scale models with different heights of the air chamber can be extrapolated on the basis of that height. In small scale models, the compressibility effects are difficult to be separated from other scaling effects related to skin friction, boundary layer and surface tension. Therefore, the proposed method can be considered an holistic approach. An application of this methodology and its related scale effects are investigated in the following sections.

### 3. Modelling setup

Physical modelling of an OWC system is a complex task since it involves at the same time wave-structure interaction, air compressibility and PTO dynamics. A simplified approach is here followed, in which the PTO is substituted by an orifice.

The reference modelling setup, shown in Fig. 1, is a generalized OWC placed at the top of a ramp, which was tested at the Large Wave Channel (GWK) of the Coastal Research Centre (FZK) in Hannover (Allsop et al., 2014). Such a large scale model was approximately 1:5 to 1:9 of full scale and it was equipped with wave gauges, pressure sensors, differential pressure transducer and air flow propeller. Data was registered by such sensors at a frequency of 1000 Hz and it was analysed by Viviano et al. (2016) under random wave conditions, by considering wave reflection and loadings. A first analysis allowed to define the optimum orifice as the most efficient flow restriction, which gave the lowest reflection coefficient.

On the basis of such a generalized OWC large scale model, new small scale experiments have been carried out at the University of Catania (CT), in a sector of the wave flume which is 18 m long, 0.90 m deep and 1 m wide (see Fig. 2). Such a sector corresponds to a partition of a wider channel, which is 3.60 m large. The flap-type wave maker can reproduce random waves on the basis of an input spectrum. The scale factor between large-GWK and small-CT models is 18. Therefore, the OWC tested in the CT laboratory is about 1:90 to 1:160 of the full scale.

The OWC devices tested in small scale are constituted by a single steel box with 10 internal longitudinal dividing sheets, which

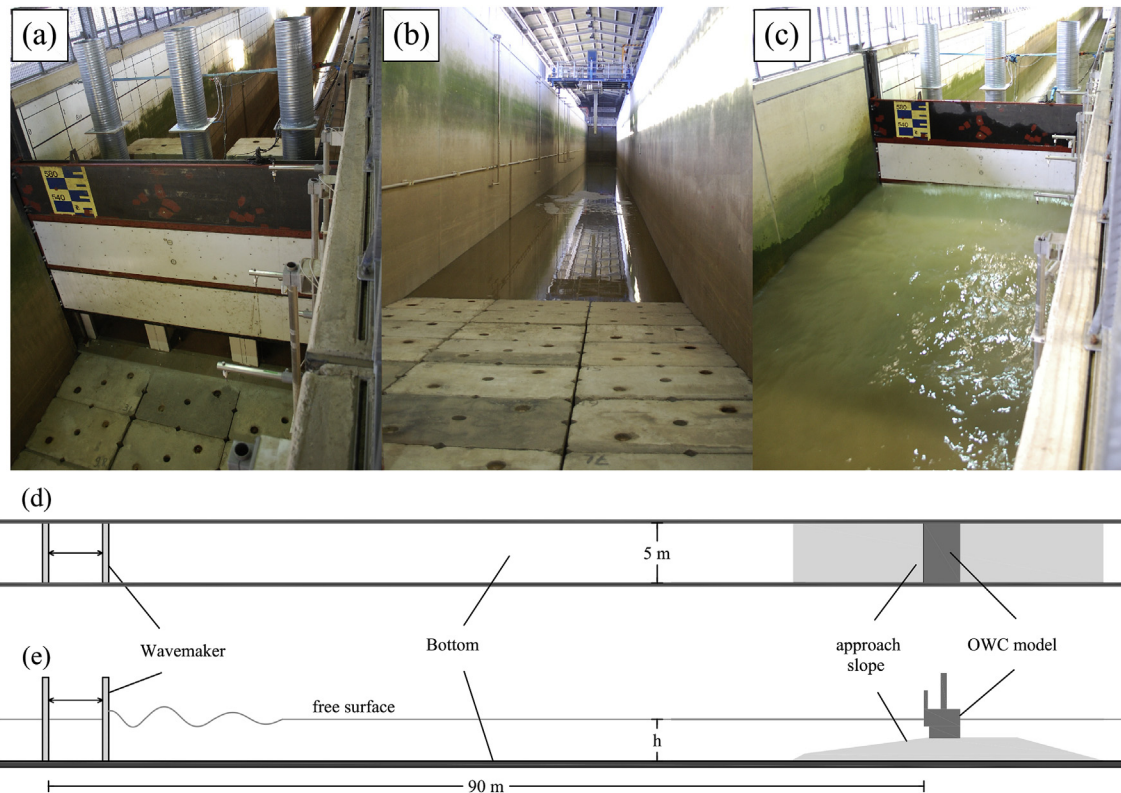


Fig. 1. Test setup and sketch of the wave flume at the Coastal Research Centre in Hannover (GWK) with the large scale OWC model: (a-b-c) photos of the setup (from Viviano et al., 2016); (d) top view; (e) longitudinal section.

constitutes 11 chambers (see Fig. 3). The front vertical sheet is cut at the bottom so obtaining the chamber opening. The top of each chamber is covered by a pierced horizontal sheet, curved at its edges, which can be fixed at different heights on the front and rear sheets by means of bolts. A tube with internal restriction (i.e. an orifice) is fixed above each horizontal top sheet, in order to simulate the PTO.

The new small scale experiments have been carried out by considering the geometrical parameters summarized in Table 1 (viz. column CT). All the linear dimensions have been scaled by dividing for the same factor  $\epsilon = 18$  the corresponding dimension of the GWK large scale model with optimum orifice. The slope of the ramp ( $s= 1:6$ ) is the same in the two models.

The system adopted in CT-experiments allows to vary the top of the OWC, thus two small scale models have been tested having

different height of the chamber  $h_t$ : (i) low-chamber CT-model having  $h_t = 0.13$  m, which corresponds to the exact geometric scale of the GWK-model; (ii) high-chamber CT-model with  $h_t = 0.28$  m; such a value approximately quintuples the height of the air volume ( $h_a = h_t - d$ ) with respect to the low-chamber CT-model, i.e.  $h_a = 0.04$  m vs. 0.19 m.

Measurements have been carried out by means of six wave gauges (W1-W6) and three pressure sensors (P1-P3). Fig. 4 shows that 3 wave gauges (W1-W3) are placed along the flat part of the wave flume and are used for estimating wave reflection. Two wave gauges (W4-W5) are placed in front of the central chamber. Such a chamber, sketched in Fig. 4 (b), is equipped with the air pressure sensor P3 and with the wave gauge W6. The latter wave gauge measures internal free surface and it is inserted in the chamber through a plastic restriction which represents

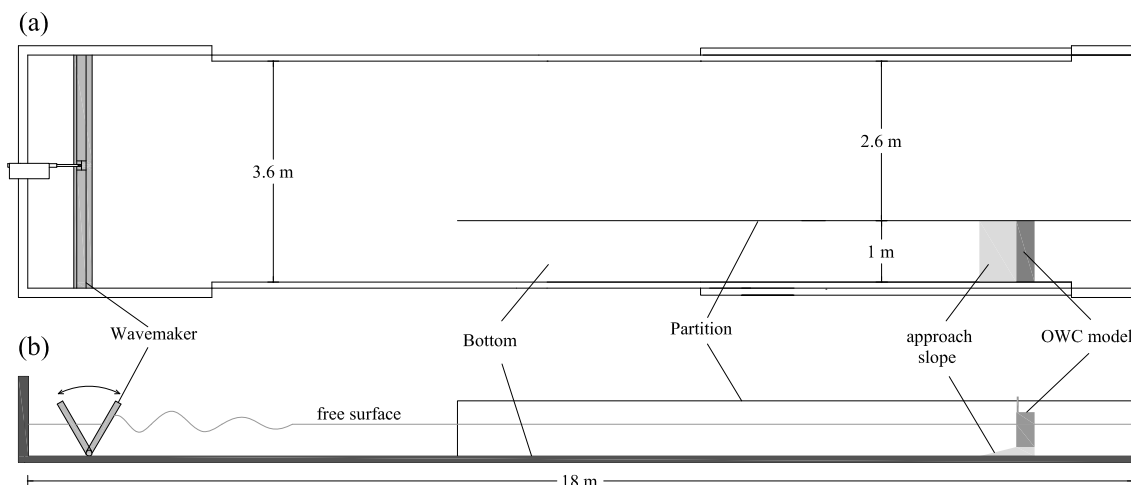


Fig. 2. Wave flume at the University of Catania (CT) with a small scale OWC model placed in a partition of the channel: (a) top view; (b) longitudinal section.

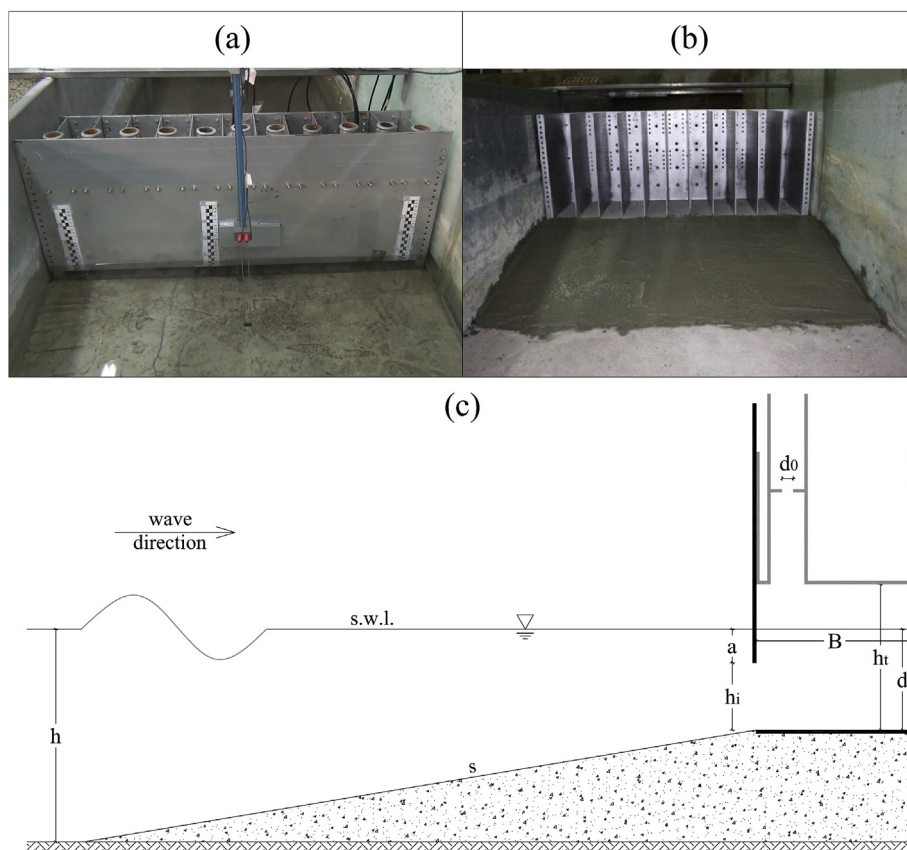


Fig. 3. Photos and sketch of the OWC small scale setup: (a) view of front wall and upper part of air ducts; (b) model under construction with its internal steel sheets and external concrete slope; (c) schematic section with main geometrical parameters.

Table 1

List of the geometrical parameters adopted in GWK large scale model (with optimum orifice) and in CT small scale tests. Two CT-models have been tested having different heights of chamber  $h_i$ .

Geometrical parameter	Symbol	GWK	CT
Approach slope	$s$	1:6	1:6
Longitudinal width of chamber	$B$	2.45 m	0.14 m
Transverse width of chamber	$B_t$	1.44 m	0.08 m
Water depth from flume floor	$h$	3.50 m	0.19 m
Water depth from chamber floor	$d$	1.58 m	0.09 m
Draft of front vertical wall	$a$	0.58 m	0.03 m
Opening height of the front wall	$h_i$	1.00 m	0.06 m
Orifice diameter	$d_0$	0.20 m	0.011 m
Height of chamber	$h_t$	2.30 m	0.13–0.28 m

the orifice.

Loadings at the outer side of the front wall are investigated by means of the pressure sensors P1 and P2, which are located inside a lateral chamber sketched in Fig. 4 (c). That setup allows to reduce the impact of the pressure sensors on the central equipped chamber.

The pressure sensors have model number ATM.1ST/N. They are fully submersible and made of stainless steel alloy 316L. Their full scale pressure is 50 mbar. The accuracy is  $\pm 0.1$  mbar, i.e.  $\pm 0.2\%$  of the full scale. The output signal is given in voltage with a sensitivity 5.0 mbar/V.

All the tests were carried out with random waves having JONSWAP spectrum and peak enhancement factor  $\gamma = 3.3$ . Nine wave conditions have been tested in both GWK and CT models, which are summarized in Table 2. Small scale CT incident wave conditions are chosen in order to follow the Froude similarity of GWK tests: (i) significant wave heights  $H_{m0,i}$  are scaled with  $\epsilon$ ; (ii) peak wave periods  $T_p$  are scaled with  $\epsilon^{0.5}$ .

Dimensionless parameters are also introduced in Table 2, which are

the relative incident wave height  $H^* = H_{m0,i}/h$ , the relative width of chamber  $B/L_p$  and the wave steepness  $s_w = H_{m0,i}/L_p$ . Those parameters are function of wave height, water depth  $h$ , width of chamber  $B$  and local wave length  $L_p$ ; the latter is obtained from  $T_p$  and  $h$  by applying dispersion relation. Dimensionless groups  $Fr$  and  $Re$  have been obtained by applying eqs. (2) and (3) respectively. In those equations, the characteristic velocity  $U$  has been computed on the basis of significant incident wave conditions for spectral waves, i.e.  $H_{m0,i}$  and  $T_p$ . Furthermore the characteristic length is substituted by the width of chamber  $B$ , so obtaining:

$$Fr = \frac{\pi H_{m0,i}}{T_p \sqrt{gB}} \tag{7}$$

$$Re = \frac{\pi \rho H_{m0,i} B}{\mu T_p} \tag{8}$$

All the dimensionless groups defined above allow a direct comparison between large and small scale models and are used in the following section for estimating scale effects.

#### 4. Analysis of results

Measurements of free surface elevation and pressure, both inside and outside of the pneumatic chamber, allow to describe air and water fluid dynamics in three geometric conditions: i) large scale model, tested at GWK; ii) small scale model with geometry similar to the large scale model; iii) small scale model with increased height of chamber. The tests in the small scale models have been carried out at the hydraulic laboratory of Catania (CT), and they are called “low-chamber” and “high-chamber” respectively.

The data registered during such tests regard three different aspects of the interaction between waves and OWC, i.e. the flow inside the

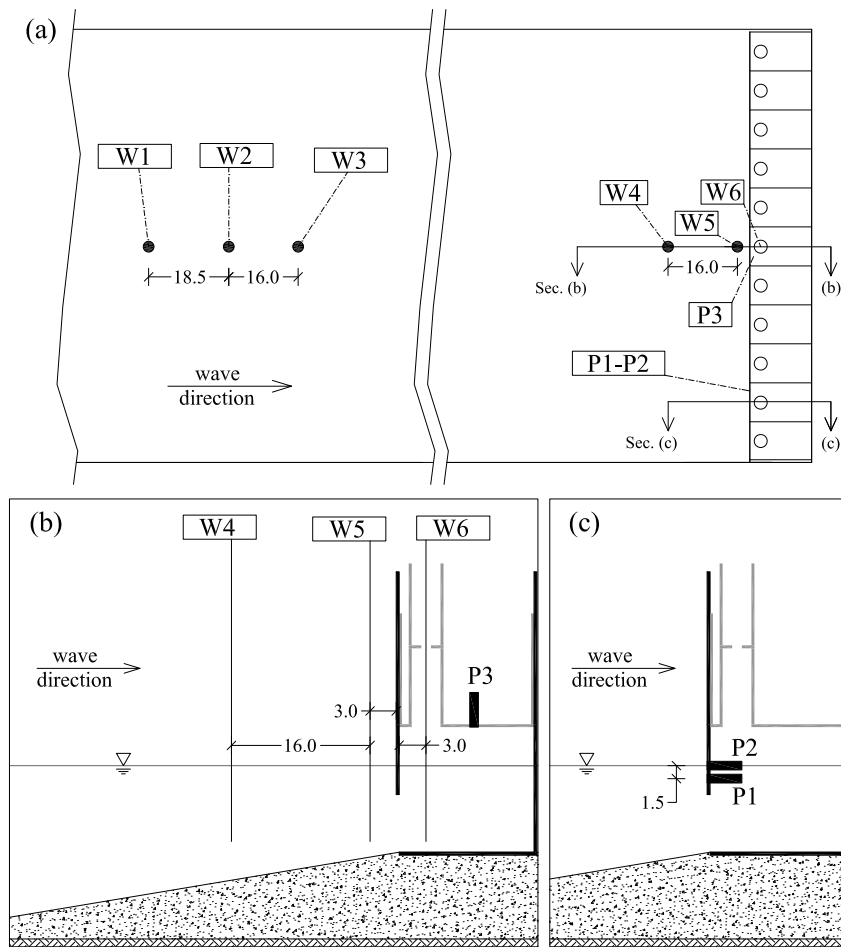


Fig. 4. Detailed views of the OWC small scale model with location of wave gauges W1-W6 and pressure sensors P1-P3: (a) top view; (b) longitudinal section crossing the central chamber where air pressure and internal water surface are registered; (c) longitudinal section across the lateral chamber which contains pressures sensors. All the dimensions are expressed in cm.

Table 2

Incident wave conditions tested at GWK an CT models;  $H_{m0,i}$  is the significant wave height;  $T_p$  is the peak wave period;  $H^* = H_{m0,i}/h$  is the relative wave height;  $B/L_p$  is the relative width of chamber;  $s_w = H_{m0,i}/L_p$  is the wave steepness;  $Fr$  and  $Re$  are function of  $H_{m0,i}$ ,  $T_p$  and width of chamber  $B$ .

Index	$H_{m0,i}$ [m]	$T_p$ [s]	$H^*$	$B/L_p$	$s_w$	$Fr$	$Re$
GWK1	0.40	4.0	0.11	0.12	0.016	0.064	$7.70 \cdot 10^5$
GWK2	0.54	5.0	0.15	0.09	0.014	0.069	$8.31 \cdot 10^5$
GWK3	0.40	6.5	0.11	0.07	0.006	0.039	$4.74 \cdot 10^5$
GWK4	0.39	3.0	0.11	0.19	0.028	0.083	$1.00 \cdot 10^6$
GWK5	0.52	3.0	0.15	0.19	0.037	0.111	$1.33 \cdot 10^6$
GWK6	0.60	4.0	0.17	0.12	0.024	0.096	$1.15 \cdot 10^6$
GWK7	0.80	4.0	0.23	0.12	0.032	0.128	$1.54 \cdot 10^6$
GWK8	0.81	5.0	0.23	0.09	0.021	0.104	$1.25 \cdot 10^6$
GWK9	1.00	6.0	0.29	0.08	0.018	0.107	$1.28 \cdot 10^6$
CT1	0.02	0.9	0.11	0.13	0.016	0.060	$9.77 \cdot 10^3$
CT2	0.03	1.2	0.16	0.09	0.013	0.067	$1.10 \cdot 10^4$
CT3	0.02	1.5	0.11	0.07	0.006	0.036	$5.86 \cdot 10^3$
CT4	0.02	0.7	0.11	0.19	0.026	0.077	$1.26 \cdot 10^4$
CT5	0.03	0.7	0.16	0.19	0.039	0.115	$1.88 \cdot 10^4$
CT6	0.03	0.9	0.16	0.13	0.024	0.089	$1.47 \cdot 10^4$
CT7	0.04	0.9	0.21	0.13	0.032	0.119	$1.95 \cdot 10^4$
CT8	0.05	1.2	0.26	0.09	0.022	0.112	$1.83 \cdot 10^4$

chamber, the wave reflection and the loadings at the front wall. Such phenomena are here investigated for all the models described above, and the results are compared each other in order to discuss their differences.

#### 4.1. Hydrodynamics of the water column

The flow inside the chamber is related both to the OWC geometry and to the incident wave conditions. In particular, the volume of air inside the chamber and the PTO play a key role in the hydrodynamics of the water column but it is difficult to analyse all those aspects separately, above all in the small scale. Therefore, an holistic approach has been followed here by investigating the eigen period of the water column. Such a procedure was proposed by Boccotti (2007), who related the resonance period of the device with the time lag between the flow inside the chamber  $q$  and the wave pressure  $\Delta p$  on the outer opening of the chamber, i.e. at the lowest part of the front wall.

In the presence of random waves, both  $q$  and  $\Delta p$  are not periodic but they can be expressed as sum of periodic components. Therefore, a cross correlation can be computed for estimating their time lag:

$$\Psi(T) = \langle \Delta p(t)q(t + T) \rangle \tag{9}$$

where the angle brackets denote an average over the time. The natural period of the plant is called here  $T^*$  and it is equal to 4 times the delay  $T$  for which the maximum of  $\Psi(T)$  is achieved (see Arena et al., 2015).

If the peak period is near to the natural period, the device works near to the resonance condition, and such a condition allows to achieve

the maximum rate of energy conversion.

The natural period of the device is mainly function of the pneumatic chamber dimension. Therefore, its comparison with a characteristic length of the device (i.e. the chamber width  $B$ ) needs for the definition of a dimensionless resonance period  $\hat{T}$ , defined as follows

$$\hat{T} = T^* \sqrt{\frac{g}{2\pi B}} \tag{10}$$

The results of the tests carried out both in small scale and in large scale are shown in Fig. 5 in terms of the dimensionless resonance period as a function of the Froude number defined in eq (7). For each geometry and scale tested, it is possible to define a horizontal asymptote for increasing values of  $Fr$ . Such a tendency is better highlighted by means of the hyperbolic interpolations. The small scale CT-tests have asymptotic values of  $\hat{T}$  higher than those of the large scale GWK-tests. That result highlights a first scaling issue which involves a different response to incident wave motion between the large and the small scale models. Such a scale effect may have multiple reasons, mainly related to differences in: (i) water motions and (ii) air compressibility inside the chamber, (iii) air in- and out-flow through the orifice. The differences in the water motion inside the chamber are likely the most important effect. They are related to the higher rate of energy losses in the small scale, which reduces the velocity of the fluid inside the chamber and increases the natural period of the water column oscillations. The causes of those greater losses in the small scale are the differences in Reynolds number and in surface tension between large and small scale models.

The variation of the chamber height causes small effects on the natural oscillation period. In particular, the asymptotic value of  $\hat{T}$  for high-chamber small scale configuration is increased of about 5% if compared with the results for the low-chamber small scale setup.

A further analysis of the chamber hydrodynamics have involved the significant height  $H_{c,m0}$ , evaluated from the mean free surface elevation inside chamber  $\bar{\eta}_c$ :

$$H_{c,m0} = 4\sigma(\bar{\eta}_c) \tag{11}$$

where  $\sigma$  is the standard deviation.

In order to compare data measured at different scales,  $H_{m0}$  is made dimensionless by dividing it for the flume water depth  $h$ . Fig. 6 shows

such a relative height inside the chamber as a function of the incident relative wave height  $H^*$  for the all the tests carried out. The results are quite confusing for small incident heights, since the effect of the wave period dominates. On the contrary, an increasing trend is present when  $H^* > 0.2$ . In such a range, it is possible to note that the free surface motion inside the GWK large-scale model has a trend which stays in between the high-chamber and low-chamber small-scale models.

#### 4.2. Wave reflection

The effect of an OWC plant on the external wave motion is analysed here, by separating the incident and reflected wave components. Since the waves are random, a spectral decomposition has been carried out on the free surface elevations registered at the wave gauges W1, W2 and W3 shown in Fig. 4. On the basis of those wave spectra, the incident and reflected components are estimated by means of the three probe method formulated by Mansard and Funke (1980). Such a method was compared, in Viviano et al. (2016), with the more reliable four probe method proposed in Faraci et al. (2015), obtaining good agreements for all the wave conditions tested in the large scale OWC model. Therefore, the three probes method can be considered reliable also for the tests carried out in the small scale with similar wave conditions.

For each test, the applied method of decomposition provides the incident and reflected wave energy spectra as a function of the frequency  $f$  of each wave component. Such a procedure allows to analyse both the total reflection coefficient  $C_r$  and the frequency-related reflection coefficient  $C_{r(f)}$ .  $C_r$  is the square root of the ratio between the integrals of the reflected and incident wave spectra;  $C_{r(f)}$  is a function of the frequency, and it is defined as the ratio between the reflected and the incident wave amplitudes for each value of  $f$ .

The values of  $C_r$  are shown in Fig. 7 for all the tests carried out in small and large scale configurations, as a function the dimensionless parameter  $B/L_p$ . The most evident result is that the small scale experiments provide values of  $C_r$  lower than those of the large scale tests. The increase in chamber height causes a slight growth of the reflected waves. Furthermore, a linear extrapolation has been carried out of the reflection coefficient obtained in the small scale configurations, by considering the height of the air volume inside the pneumatic chamber in still water condition, i.e.  $h_a$ . On the basis of the dimensional analysis,

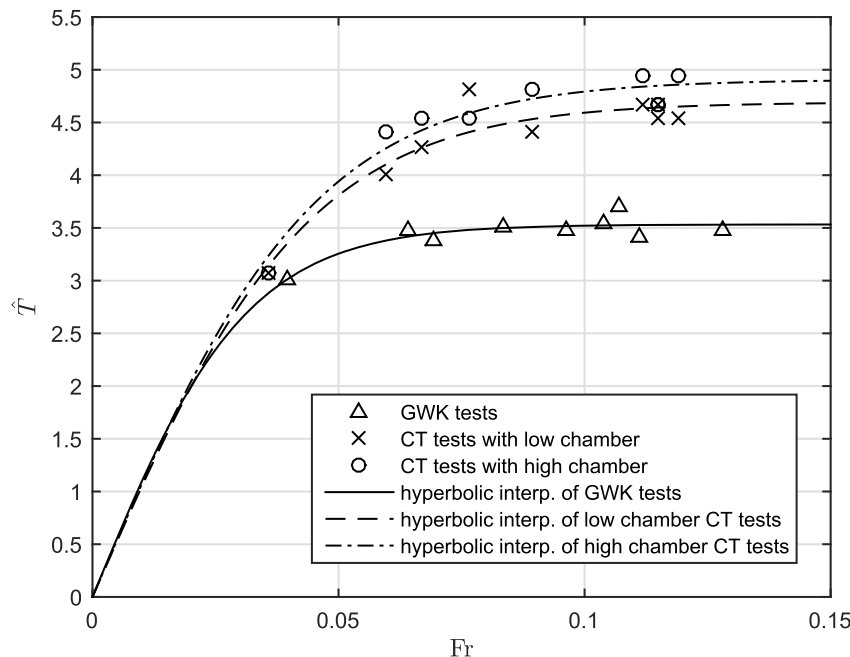


Fig. 5. Dimensionless resonance period  $\hat{T}$  of the device as function of the Froude number of incident waves; results of the large scale GWK-tests and small scale CT-tests with interpolation lines.

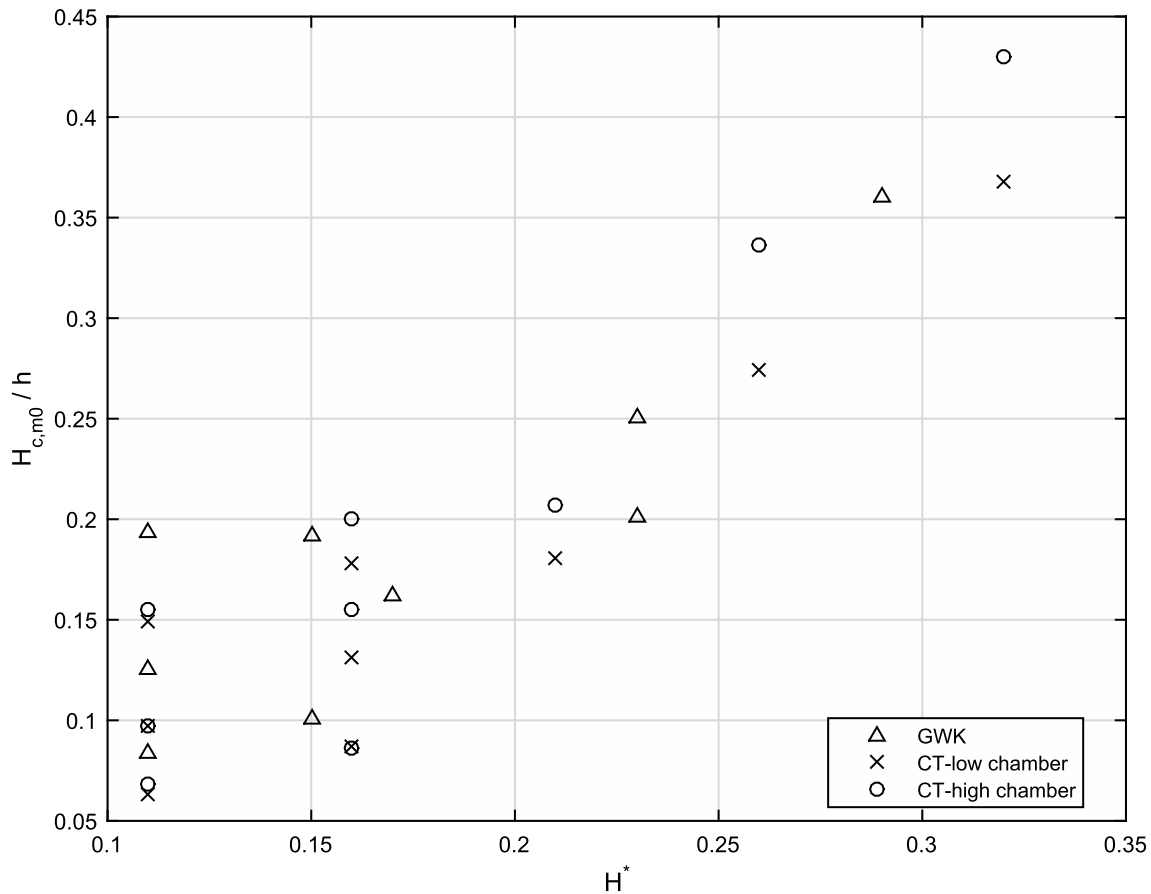


Fig. 6. Significant relative wave height inside the chamber  $H_{c,m0}/h$  versus the significant incident relative wave height  $H^*$ . Results of the GWK-model are compared with the low- and high-chamber CT-models.

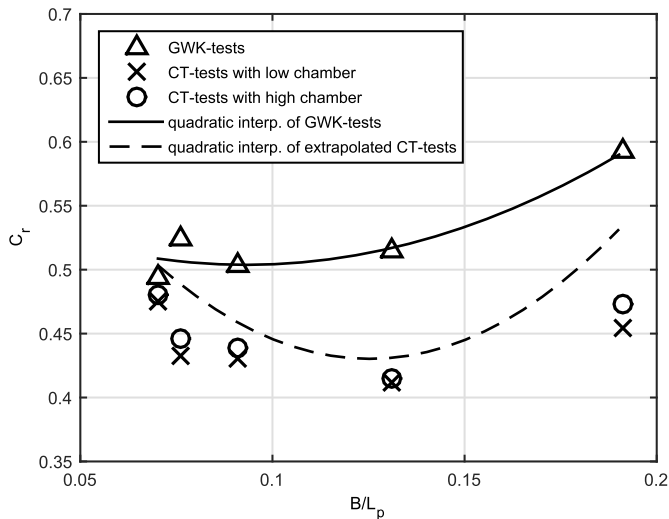


Fig. 7. Reflection coefficient  $C_r$  as function of relative width of chamber  $B/L_p$  for large scale GWK-tests and small scale CT-tests. Results for low-chamber and high-chamber small scale tests are used to extrapolate values of  $C_r$  for height of air chamber equal to that of large scale model. Quadratic interpolations are related to large-scale and to extrapolated small-scale results.

the correct way to scale the OWC device would be by keeping constant  $h_a$ , which assumes the value 0.72 m in the large scale model. Therefore, the extrapolation of the small scale models have been carried out by considering such a value of  $h_a$ .

Fig. 7 shows that the extrapolation allows to increase the reflection

coefficients obtained in the small scale setups. Nevertheless, the values of  $C_r$  obtained in the large scale model are still greater than those extrapolated from the small scale tests. Such a difference is more evident for a relative width of chamber  $B/L_p = 0.1-0.15$ . Those values of  $B/L_p$  corresponds to dimensionless peak wave periods  $T_p \sqrt{g/(2\pi B)}$  close to the resonance dimensionless period  $\hat{T}$  found in the previous section. Thus the scale effects are more prominent on wave reflection for incident waves having the peak period close to the natural oscillation period of the OWC. Therefore, the small scale models give the greatest errors when the device works near to the resonance, with a maximum reduction of the reflection coefficient of about 20% in comparison with the large scale configuration.

The variation of the orifice thickness ( $\delta$ ) can also play a role on the result obtained at different scales.

In particular, a distinction between thin and thick wall orifices can be considered (see Fossa and Guglielmini, 2002; He and Huang, 2014): openings with  $\delta/d_0 < 0.5$  are classified thin openings; instead, those with  $\delta/d_0 > 0.5$  are called thick openings. In the large-scale GWK model, the orifice was executed in a layer having  $\delta = 2$  cm. Such a thickness was not scaled geometrically in the CT models, indeed  $\delta = 0.5$  cm in the small scale. The resulting ratio  $\delta/d_0$  is then 0.10 and 0.45 in the GWK and CT models respectively. As a consequence, is possible to affirm that such a variation of thickness does not affect appreciably their results. Indeed, the orifice dimensions fall in the thin wall case ( $\delta/d_0 > 0.5$ ) in the large and small scale models.

The scale effects on the reflected wave spectrum are investigated here by focusing on the mean spectral reflection coefficient  $\overline{C_{r(f)}}$ , which is defined for each frequency  $f$  as the average of  $C_{r(f)}$  for all the wave conditions tested in the experiments. Fig. 8 shows  $\overline{C_{r(f)}}$  as a function of the relative width of chamber  $B/L$  for the large scale



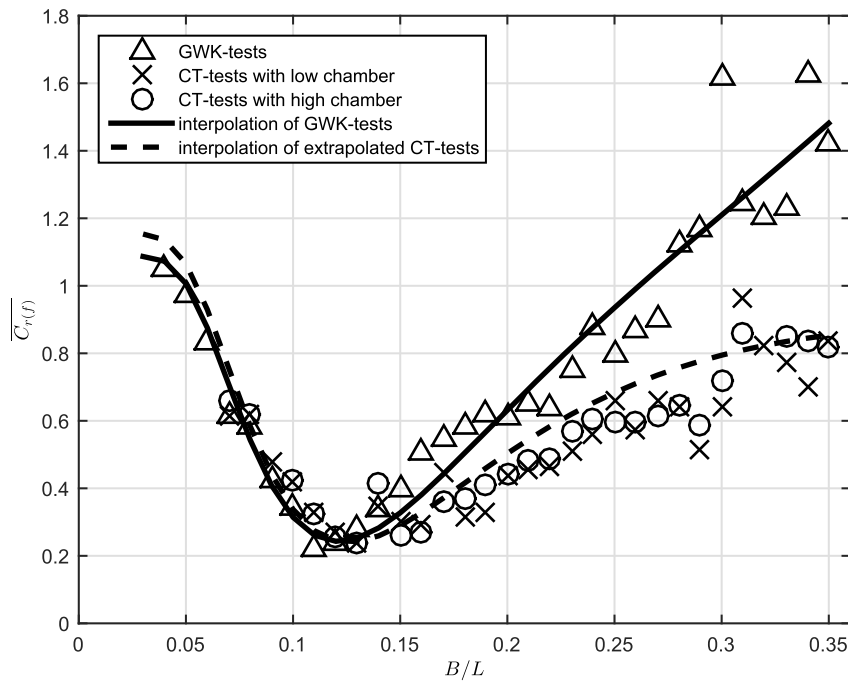


Fig. 8. Mean spectral reflection coefficient  $\overline{C_{r(f)}}$  as function of relative width of chamber  $B/L$  for large scale GWK-tests and for small scale CT-tests with low and high chamber. Interpolating functions are plotted for large scale and for extrapolated small-scale results, by considering an height of air chamber equal to that of large scale model.

GWK-tests and for the small scale CT-tests with low and high chamber. Furthermore, the interpolation function of  $\overline{C_{r(f)}}$  is determined on the extrapolated values of CT-tests, similarly to what has been done for  $C_r$ . The resulting extrapolated function  $\overline{C_{r(f)}}$  from the small scale configurations is close to the values obtained for the large scale model for  $B/L < 0.15$ , i.e. for wave period greater or equal to the natural oscillation period of the water column. Notwithstanding the extrapolation, the small

scale models furnish values of  $\overline{C_{r(f)}}$  smaller than the large scale tests for wave components having period smaller than the natural oscillation period. In particular,  $\overline{C_{r(f)}} > 1$  for  $B/L > 0.3$  in the large scale tests, thus the energy is shifted from smaller toward higher  $B/L$ . Such a result is not related to a single wave conditions but it is the effect of the air-water interaction inside the chamber. That effect is considerably reduced in the small scale models since  $\overline{C_{r(f)}}$  is always lower than 1, and the reflected

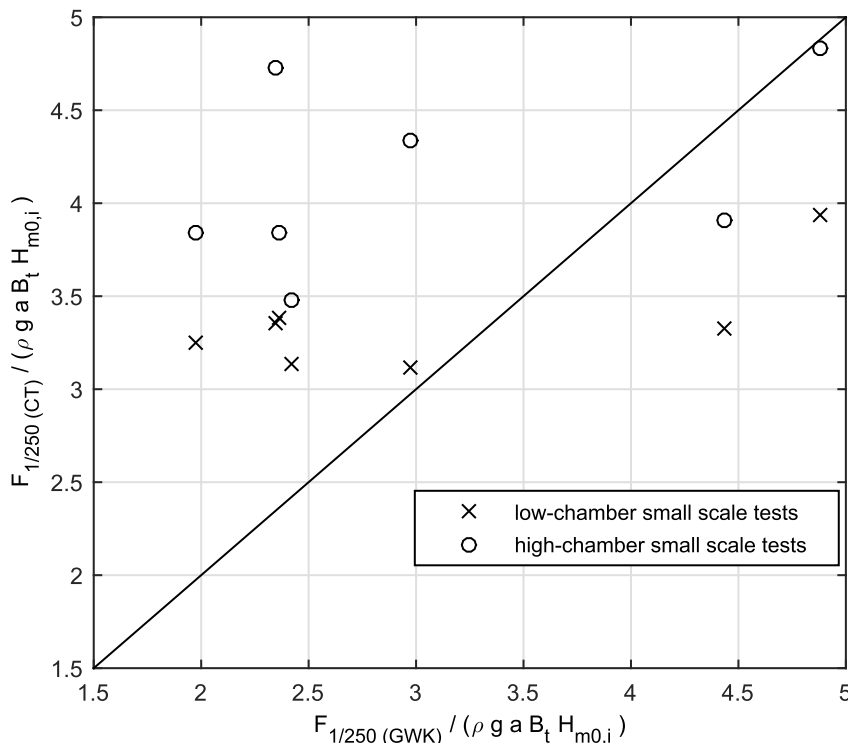


Fig. 9. Dimensionless maximum (1/250) force acting on the front wall for large scale GWK-tests and for small scale CT-test. The latter tests are reported by considering configurations with low and high roof of the pneumatic chamber.

wave components are always lower than those incident.

The obtained discrepancy between the large and the small scale models may have multiple causes. Indeed, the Reynolds numbers are lower than  $10^5$  in the small-scale models and the viscosity can play a role on the scale effects. Furthermore, the stiffness of the chamber have been varied from the large to the small scale, due to the use of concrete and steel, respectively. All those issues are common in scaling OWC devices. They cause an excessive energy damping in the small scale, which affect both the resonant period and the wave reflection.

#### 4.3. Loadings

The most critical structural point of the OWC caissons is the front wall, due to the interaction between incident waves and oscillating motion from the pneumatic chamber. Therefore, the attention has been focused here on the loadings registered at the outer part of the front wall.

In both large and small scale laboratories, the pressures have been registered with a frequency of 1000 Hz, in order to measure the peaks of impulsive loadings. The pressures registered at the front wall along a vertical direction represent the pressure profile. The integral of such a profile furnishes the force per unit length of front wall, defined as  $F/B_f$ , where  $F$  is the force acting on each OWC caisson having transverse width  $B_f$ .

Starting from the time series of the force related to 1000 waves, the 4 highest values are averaged in order to have the  $1/250$  maximum force, called  $F_{1/250}$ . In order to compare results from different scales, a dimensionless variable is used which is obtained by dividing  $F_{1/250}$  for the term  $\rho g a B_f H_{m0,i}$ .

Fig. 9 shows the comparison between the dimensionless maximum forces obtained from large and small scale experiments, with indication of those tests carried out with different height of the chamber. It is evident that the results from the small scale models provide dimensionless forces quite constant in comparison with the large scale model. This is a direct effect of the viscous stresses which modify the hydrodynamics inside the OWC by reducing flow velocity near the wall.

#### 5. Discussion on the effects of changing the air chamber height

The experiments carried out at the small-scale facility furnishes the possibility of investigate the effect of varying the air chamber volume inside the OWC by means of the height of its roof. The results reported in the previous section have showed that such a variation does not reduce the scale effects at a great extent. Nevertheless, the changing of the air volume involves several changes in the system dynamics which need to be discussed and related each other.

Since the horizontal section of the OWC has been unchanged during the experiments, the variation of the height of the air chamber  $h_a$  is proportional to the air volume. In the so called small-scale models, the ratio between the two values of  $h_a$  (and of air volume) tested was 4.75.

The increase in chamber height affects the air water dynamics inside the device by means of the increase of both the natural period and the significant wave height measured inside the chamber, as shown in Figs. 5 and 6 respectively.

The natural period is increased weakly (lower than 10%) but quite uniformly along the tests carried out with greater  $h_a$ . The rationale behind such a behaviour is that when the volume of air increases, the water column is less opposed by the air pressure. Therefore, the presence of a greater air volume inside the pneumatic chamber acts like a weaker spring, which increases the natural oscillation period of the water column with respect to the low-chamber configuration. Such a phenomenon acts independently from the characteristics of incident waves, i.e. from the internal excursion of the free surface. As a consequence, the oscillation phase response of the system acts like a linear phenomenon, which is independent from the amplitudes.

The analysis of wave loadings on the front face highlights that the

small scale setup with high chamber provides a fairly good match with the large scale setup for the most violent storms. The rationale of such a behaviour is related to what has been inferred above; indeed, the increase of air volume inside the pneumatic chamber causes a lower opposition to the water column oscillations due to air compressibility. The resulting greater oscillations inside the chamber cause, in turn, the increase of both wave height and force at the external side of the front wall.

#### 6. Conclusions

The main issue related to the physical modelling of an OWC is the air-water interaction inside the pneumatic chamber. Indeed, the volume of air in that chamber needs to be scaled differently from the rest of the device, possibly by maintaining its height. Unfortunately, it is difficult to achieve in the small scale models; the modelling system adopted here allows to vary such a height in order to quantify its effect on the behaviour of the modeled device.

The similitude is achieved by maintaining constant the parameter  $Fr$ , so obtaining a Froude similarity. The turbine scaling is not considered in the present study, since the power take off has been substituted with an orifice in both large and small scale models. Furthermore, the scale effects related to the thickness variation of such orifices can be neglected from a comparison with the available literature data.

Measurements of water column oscillations inside the pneumatic chamber allow to obtain the natural period of the device, which is proportionally greater in the small scale than in the large scale. An increase in chamber height causes a further increment of the natural oscillation period, which diverges from that obtained in the large scale model. Therefore, the increment of the air volume in the pneumatic chamber appears to increase the scale effects on the internal hydrodynamics of the OWC. The rationale is that the viscous stresses in the small scale cause a greater reduction of flow velocity in comparison with the large scale. Such a phenomenon, in turns, increases the natural period of the small scaled device rather than reducing it, as it would be expected due to the low-chamber condition. For the high-chamber tests, the natural oscillation period increases further the effect of air compressibility which acts like a weaker spring due to the higher volume of air.

The amplitude of the free surface motion inside the pneumatic chamber shows that the large scale model has a behaviour more similar to the high-chamber than to the low-chamber small scale configuration. Such a behaviour is realistically related to the air compressibility, since the viscosity distortion due to the differences in Reynolds numbers act similarly in the two small scale models.

The increased height of chamber is beneficial in reducing scale effects on the reflection coefficient  $C_r$ . Indeed, the small scale tests give a lower reflection effect than the large scale tests and the increase in height of chamber causes values of  $C_r$  which are closer to those obtained from the large scale model. Nevertheless, the increase in height of chamber is not sufficient for overcoming scale effects, especially when the device works near to resonance. The analysis of the frequency-related reflection highlights the absence of a strong redistribution of energy through wave components having different frequencies, as opposed to what happens in the large scale. Such a different behaviour is again related to the pneumatic chamber which has a weak effect in the small scale models, also for the high-chamber configuration.

It is important to stress that the adopted geometrical scaling procedure by itself does not assure a similar response between the small-scale and the large-scale models. Indeed, the dimensionless resonance period of the system can be also 40% greater in the small-scale. Thus, the small-scaled OWC might respond differently to the incident wave spectra near to the resonant condition, i.e. when the device provides a maximum of energy conversion and a minimum of wave reflection. Nevertheless, the mean spectral reflection coefficients highlight a

similar behaviour between the small-scale and the large-scale tests towards their minimum values, i.e. at the optimum conditions. Therefore, the increase of dimensionless resonance period does not affect the response of the small-scale model to the incident wave spectra.

The comparison of dimensionless maximum (1/250) forces at the outer front wall between large and small scale models highlights a different behaviour, due to the presence of viscous stresses in the latter models. For the heaviest incident wave conditions, the forces obtained for the small scale model with high chamber have a better agreement with the large scale model. Therefore, a little increase in the height of the pneumatic chamber is sufficient to provide a fairly safe prediction of the maximum loadings.

A specific analysis have been carried out on the variation of air chamber height (and volume) in the so called small-scale models. Such a variation affects weakly the wave-air interaction inside the chamber, but strongly the wave related forces at the device.

### Acknowledgement

This work has been partly funded by the EU funded project HYDRALAB PLUS (proposal number 654110), by the project “NEWS - Nearshore hazard monitoring and Early Warning System” (code C1-3.2-60) in the framework of the programme INTERREG V-A Italia Malta 2014-2020, and by University of Catania funded project “Interazione ondecorrenti nella regione costiera (INOCS)”.

### References

- Allsop, W., Bruce, T., Alderson, J., Ferrante, V., Russo, V., Vicinanza, D., Kudella, M., 2014. Large scale tests on a generalised oscillating water column wave energy converter. In: Proceedings of the HYDRALAB IV Joint User Meeting, Lisbon.
- Arena, F., Laface, V., Malara, G., Strati, F., 2015. Optimal configuration of a U-OWC wave energy converter. In: Guedes Ssoares, C. (Ed.), Renewable Energies Offshore. CRC Press, pp. 429–436.
- Boccotti, P., 2007. Caisson breakwaters embodying an OWC with a small opening - Part I: Theory. *Ocean. Eng.* 34, 806–819.
- Carballo, R., Iglesias, G., 2012. A methodology to determine the power performance of wave energy converters at a particular coastal location. *Energy Convers. Manag.* 61, 8–18.
- Dean, R., Dalrymple, R., 1991. *Water Wave Mechanics for Engineers and Scientists*. World Scientific, Singapore.
- Falcao, A.F., Henriques, J.C., 2016. Oscillating-water-column wave energy converters and air turbines: a review. *Renew. Energy* 85, 1391–1424.
- Falcao, A.F.O., Henriques, J.C.C., 2014. Model-prototype similarity of oscillating-water-column wave energy converters. *Int. J. Mar. Energy* 6, 18–34.
- Faraci, C., Scandura, P., Foti, E., 2015. Reflection of sea waves by combined caissons. *J. Waterw. Port. Coast. Ocean Eng.* 141 (2) 04014036.
- Fleming, A., Macfarlane, G., 2017a. Experimental flow field comparison for a series of scale model oscillating water column wave energy converters. *Mar. Struct.* 52, 108–125.
- Fleming, A., Macfarlane, G., 2017b. In-situ orifice calibration for reversing oscillating flow and improved performance prediction for oscillating water column model test experiments. *Int. J. Mar. Energy* 17, 147–155.
- Fleming, A., Penesis, I., Macfarlane, G., Bose, N., Denniss, T., 2012. Energy balance analysis for an oscillating water column wave energy converter. *Ocean. Eng.* 54, 26–33.
- Fossa, M., Guglielmini, G., 2002. Pressure drop and void fraction profiles during horizontal flow through thin and thick orifices. *Exp. Therm. Fluid Sci.* 26, 513523.
- He, F., Huang, Z., 2014. Hydrodynamic performance of pile-supported owc-type structures as breakwaters: an experimental study. *Ocean. Eng.* 88 (Suppl. C), 618–626.
- Iuppa, C., Cavallaro, L., Foti, E., Vicinanza, D., 2015a. Potential wave energy production by different wave energy converters around sicily. *J. Renew. Sustain. Energy* 7 (6).
- Iuppa, C., Cavallaro, L., Vicinanza, D., Foti, E., 2015b. Investigation of suitable sites for wave energy converters around Sicily (Italy). *Ocean Sci.* 11 (4), 543–557.
- Lopez, I., Pereiras, B., Castro, F., Iglesias, G., 2016. Holistic performance analysis and turbine-induced damping for an OWC wave energy converter. *Renew. Energy* 85, 1155–1163.
- Mahnamfar, F., Altunkaynak, A., 2016. OWC-type wave chamber optimization under series of regular waves. *Arabian J. Sci. Eng.* 41 (4), 1543–1549.
- Mahnamfar, F., Altunkaynak, A., 2017. Comparison of numerical and experimental analyses for optimizing the geometry of OWC systems. *Ocean. Eng.* 130, 10–24.
- Mansard, E., Funke, E., 1980. The measurement of incident and reflected spectra using a least squares method. In: Proc. 17th Int. Coastal Engineering Conf., ASCE, New York, pp. 154–172.
- Mitchell Ferguson, T., Penesis, I., Macfarlane, G., Fleming, A., 2017. A PIV investigation of OWC operation in regular, polychromatic and irregular waves. *Renew. Energy* 103, 143–155.
- Naty, S., Viviano, A., Foti, E., 2016. Wave energy exploitation system integrated in the coastal structure of a mediterranean port. *Sustainability* 8 (12).
- Rezanejad, K., Soares, C.G., Lopez, I., Carballo, R., 2017. Experimental and numerical investigation of the hydrodynamic performance of an oscillating water column wave energy converter. *Renew. Energy* 106, 1–16.
- Sheng, W., Alcorn, R., Lewis, T., 2014. Physical modelling of wave energy converters. *Ocean. Eng.* 84, 29–36.
- Sheng, W., Lewis, A., 2016. Wave energy conversion of oscillating water column devices including air compressibility. *J. Renew. Sustain. Energy* 8, 054501.
- Viviano, A., Naty, S., Foti, E., Bruce, T., Allsop, W., Vicinanza, D., 2016. Large-scale experiments on the behaviour of a generalised oscillating water column under random waves. *Renew. Energy* 99, 875–887.
- Vyzikas, T., Deshoulieres, S., Barton, M., Giroux, O., Greaves, D., Simmonds, D., 2017. Experimental investigation of different geometries of fixed oscillating water column devices. *Renew. Energy* 104, 248–258.
- Weber, J.W., 2007. Representation of non-linear aero-thermodynamic effects during small scale physical model of OWC WECs. In: Proceeding of the 7th European Wave and Tidal Energy Conference.
- Wilcox, D., 1997. *Basic Fluid Mechanics*. DCW Industries.